energies

MDPI

Article

Overcoming the Limits of the Charge Transient Fault Location Algorithm by the Artificial Neural Network

Roberto Benato [1,*], Giovanni Rinzo [1] and Michele Poli [2]

[1] Department of Industrial Engineering, University of Padova, 35131 Padova, Italy; giovanni.rinzo@phd.unipd.it
[2] Terna Rete Italia, 00156 Roma, Italy; michele.poli@terna.it
* Correspondence: roberto.benato@unipd.it

Received: 11 December 2018; Accepted: 16 February 2019; Published: 22 February 2019

check for updates

Abstract: In this paper, two algorithms for single-ended fault location are presented with reference to the unearthed sub-transmission Italian grid (with a voltage level of 60 kV). Both algorithms deal with the correlation between the ground capacitance charging frequency of sound phases and the fault position. In the former, the frequency response of a lumped parameter circuit in the Laplace domain is linked to the fault distance. With such a simplified lumped parameter circuit, the average error in locating a phase-to-ground (PtG) short circuit is 5.18% (total overhead line length equal to 60 km). Since this error is too high, another approach is presented. In this second algorithm, the frequency spectra of the transient current waveforms are used as a database for the training of an Artificial Neural Network (ANN). With this approach, the average error decreases significantly up to 0.36%. The fault location accuracies of the two proposed methods are compared in order to reveal their strengths and weaknesses. The developed procedures are applied to a single-circuit overhead line and to a double-circuit one, both modelled in the EMTP-rv environment, whereas the fault location algorithms are implemented in the MATLAB environment (for the ANN-based algorithm, the Deep Learning toolbox is used).

Keywords: Artificial Neural Network; charge transient; fault location; lumped parameters circuit

1. Introduction

In the Italian electric grid, about 1940 km of overhead lines (OHLs) are still operated with unearthed neutral and their voltage level is 50–60 kV. This portion of the sub-transmission grid has a radial structure and mainly consists of non-homogeneous and asymmetrical OHLs. The most common failure mode in such OHLs is porcelain insulator cracking, which causes, at the nominal voltage, a PtG short circuit with a very low current magnitude (in the rural OHL network, the short circuit current is typically lower than 30 A) [1]. This is problematic for the Italian transmission system operator (with acronym TSO), since the location and detection of the fault positions are much more difficult than in systems with earthed neutral. Furthermore, the overhead lines involved are typically located in mountainous areas, complicating the location and repairing operations. Therefore, in order to locate the faulty section, the method, currently applied by the Italian TSO (Terna), consists of visual inspections by a helicopter or by a ground vehicle: alternatively, Terna carries out an outage of the entire faulted line, with a consequent repowering span by span until the fault section is identified [2,3]. In some previous works, the authors have proposed a travelling wave-based algorithm to overcome such limitations [4,5]. Even if the accuracy is very high, the requested sample frequency appears to be an issue for practical installations, because of the high cost of the fault location systems. In order to develop some alternative solutions, two other algorithms are presented here: they are characterized by a lower sample frequency and are based on the study of a different transient phenomenon, i.e., the ground capacitance charge transient of the sound conductors. The main purpose of the present work is to investigate the same phenomenon by means of these two different approaches in order to highlight their strengths and weaknesses.

2. Technical Literature Review

The relationship between the transient frequency and the fault distance is well-known in technical literature. In [6], the information extracted from the registered fault signals allows the authors to determine the faulty line inductance, which is compared with line sequence parameters for fault distance evaluation. In [7], the un-damped frequency of the fault signal is extracted and used in a simplified lumped parameter circuit. In the present work, the authors decide to adopt a different OHL model with respect to [7] and the fault distance is computed by means of an iterative algorithm.

There are other contributions in technical literature from Finnish authors [8–10] and from Chinese ones [11]: the results from these papers are different for both the frequency and duration of the examined phenomena. The differences are due to the typologies of the electrical grids involved.

The second algorithm presented in this paper is based on the Artificial Neural Network (ANN) theory. The importance of ANN-based algorithms is growing in the scientific community, as well as for power system analysis and fault location, as witnessed by several papers [12–21]. A certain number of ANN-based algorithms have been developed in recent years. In [12], a BPNN architecture has been developed to estimate the fault position in various locations; RMS values of current and voltage samples are the input data for this network. In [13], the authors propose an impedance-type estimator by using a phase or amplitude comparison of signals. In [14], the "prony" method is used to analyse the modal information hold in the current signal by means of the travelling wave phenomenon. In [15], Josè et al. use both the three-phase currents and the energy content of the wavelet coefficients as inputs for the ANN in order to detect and locate high impedance faults in distribution systems. In [16], a fault location method based on the radial basis function ANN is presented: the method is accurate, but it fails the sensitivity analysis. In [17], Dehghani et al. combine the response of three different ANNs in order to get better results.

In the present paper, a feed forward network ANN is trained by means of the frequency spectra of the transient faulty phase currents obtained by means of electro-magnetic transient software, i.e., EMTP-rv.

3. Brief Recalls to the Charge and Discharge Transient Currents

Because of a PtG short circuit, the OHL is affected by a redistribution of the conductor voltages throughout the whole length. The electric charge stored in the ground capacitances of the faulty phase is drained off and simultaneously, the charge stored in the sound phases increases.

It is possible to study the two phenomena independently:

- The discharge current flows directly through the phase-to-ground capacitances of the faulty phase to form a loop; the inductances of the discharge circuit are very low (Figure 1), in order to obtain a faster attenuation and a higher oscillation frequency yield;
- The charging current flows through the faulty phase up to the transformer and creates a loop by means of the ground capacitances of the two sound phases [22].

In Figure 1, the charge loop (green) and the discharge loop (red) are highlighted.

In Figure 1, c_p is the per unit length (with acronym p.u.l.) phase-to-phase capacitance, c_0 is the p.u.l. phase-to-ground capacitance, d is the fault distance, ℓ_t is the phase inductance of the transformer, ℓ_f is the p.u.l. line inductance, and D the total line length.

The frequency and amplitude of these phenomena are functions of the power system characteristics (voltage, geometry, neutral point configuration, etc ...) and fault position; in fact, the inductance of both charge and discharge loops varies with fault distance.

The charge transient is a suitable option for fault location purposes; in fact, the frequency is lower and the amplitude is higher (up to 20 times) [6].

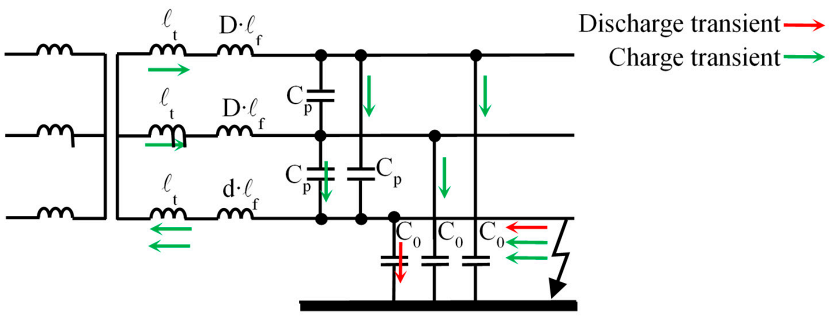

Figure 1. Charge and discharge transient circuits for a single line OHL for a PtG fault.

4. Analytical Algorithm Based on the Analysis of Charge Transient Current Waveform

The fault location procedure based on the analysis of charge transient current waveforms is shown in the flowchart of Figure 2. When a PtG occurs, firstly, it is necessary to identify the faulty feeder and the faulty phase. It is possible to apply classical or innovative algorithms for these purposes [23,24]. When the faulted phase selection process is completed, the current waveform can be properly processed by applying both the Continuous Wavelet Transform (CWT) (or alternatively the discrete Fourier Transfor (DFT)) [25] and the Hilbert Trasform (HT) [26] (see Appendix A), in order to highlight the frequency of the charge transient. [17]. As a consequence of the two subsequent transforms, the un-damped frequency f_u can be estimated. The identification of un-damped frequency is necessary since the electrical circuit which links the fault distance with the charge transient frequency is ideal or without resistances. Consequently, this circuit can give only the un-damped frequency and not the damped one. At the same time, the charge transient frequency f_c of the line model in the Laplace domain (described in Section 4.2) is calculated. The fault section can be derived by identifying the un-damped frequency in the frequency response vs the distance diagram.

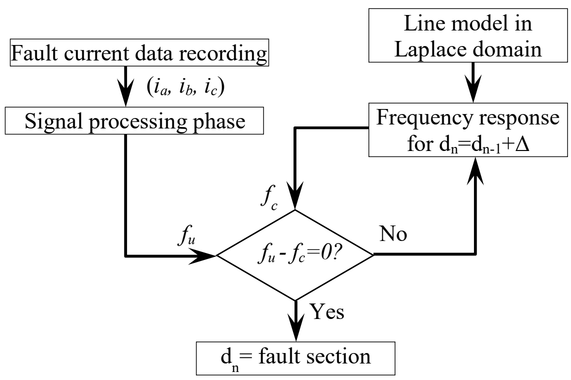

Figure 2. Flowchart of the analytical algorithm based on the analysis of charge transient current waveform.

4.1. Waveform Processing

Fault currents are composed of:

- A steady-state component, at 50 Hz;
- Some transient components, which are non-stationary with many frequency components, like noise, travelling wave propagation, charge and discharge phenomena, etc.

The main purpose of this step of the fault location algorithm consists of highlighting only the charge un-damped transient frequency, necessary for the development of the algorithm.

Firstly, it is important to remove the unwanted frequency components, like the 50 Hz one and the noise effects. This is possible by means of a classical band-pass filter [27]: in this paper, a notch filter is applied since it is a band-stop filter with a narrow stopband.

As the second step, a time-frequency analysis is applied: the choice can be the DFT or CWT. In particular, the CWT has high-resolution properties [28], whereas DFT is faster, with low CPU-times.

Figure 3 shows the results of the analysis, where charge and discharge transients are clearly highlighted by means of CWT. In Figure 3, it is clearly visible that for the charge transient, the CWT scale is greater than that pertaining to the discharge transient. Successively, in order to identify the charge transient frequency, if CWT is used, the frequency at which the maximum CWT scale occurs is derived. If DFT is used, the two-sided spectrum P2 is first computed, followed by the single-sided spectrum P1 based on P2 and the even-valued signal length frequency. By observing the single-sided amplitude spectrum of the waveform, the frequency where the maximum occurs can be immediately located. Of course, even if different CPU times are used, the two transforms (CWT and DFT) give results with negligible differences. However, detailed information about charge transient identification is reported in [7,29]. Once the charge transient signal has been identified and extracted from the entire time/frequency spectrum (*i(t)* of the faulted phase), the HT is applied to the chosen CWT scale component in order to reproduce the "pre-envelope" waveform and the un-damped frequency can be calculated. Both steps are shown in Figure 4, which firstly reports the 50 Hz filtered waveform (azure coloured waveform) and that which is successively Hilbert transformed (red coloured waveform).

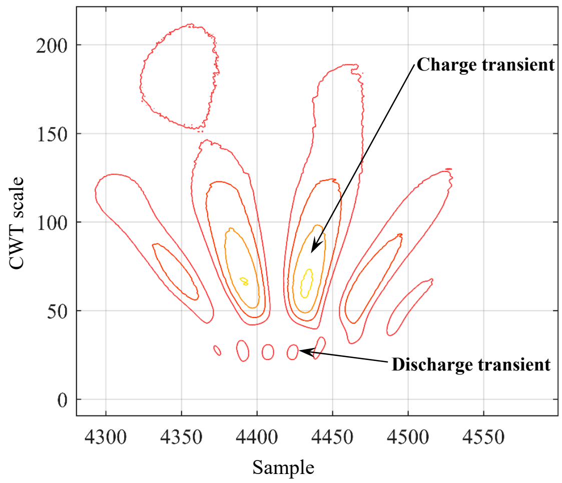

Figure 3. Contour plot of the CWT output from transient current waveform.

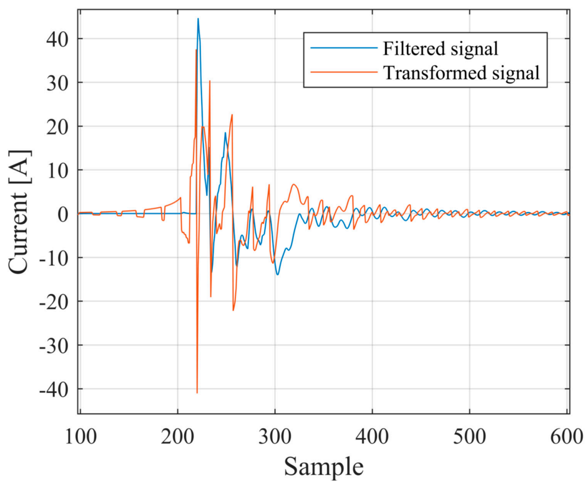

Figure 4. Filtered fault current and its Hilbert transform.

4.2. Laplace Domain Model and f_c Estimation

It is possible to model the faulted line by means of a lumped parameter circuit, as shown in Figure 5.

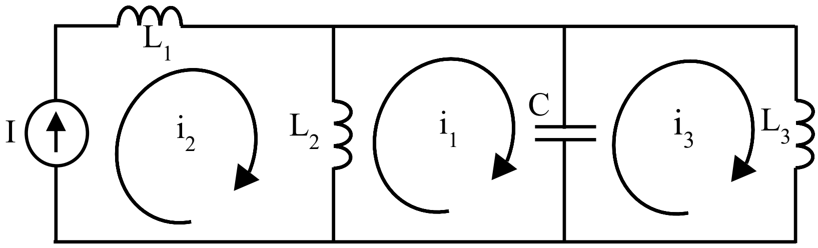

Figure 5. Charge transient circuital lumped model.

The circuit is based on the "general model 4" (also known as GM 4) presented in [30], but it is different and original for some features. GM 4 is based on parameters in a sequence frame of reference, whereas the model presented in the paper is based on parameters in a phase frame of reference. In the circuit of Figure 5, the faulty section is represented as a current generator, which imposes the fault current I. L_1 is the inductance of the faulty line from the hypothesized fault point to the substation and is equal to $d \cdot \ell_f$. L_2 is the equivalent inductance of the three-phase transformer and of the sound phases. C is the equivalent capacitance of the charge loop and L_3 the load inductance. In particular, L_2 is calculated as

$$L_2 = 1.5\ell_t + \ell_f \frac{D}{2},$$

where as C is computed as

$$C = (c_p + 2c_0) \cdot D.$$

The circuit parameters are calculated according to [30]. In C computation, it is possible to neglect the effect of the phase-to-phase capacitances between the sound phases, because from the fault current generator standpoint, they are equipotential. The circuit is solved by the voltages around loop equations, as in the following:

$$\begin{cases} i_1(s)\left(sL_2 + \dfrac{1}{sC}\right) - i_2(s)sL_2 - i_3(s)\dfrac{1}{sC} = 0 \\ -\, i_1(s)sL_2 + i_2(s)(sL_2 + sL_1) = \dfrac{E}{s} \\ -\, i_1(s)\dfrac{1}{sC} + i_3(s)\left(sL_3 + \dfrac{1}{sC}\right) = 0 \end{cases} \tag{1}$$

The characteristic Equation (1) can be found by solving the system as follows:

$$s^4 CL_2L_1L_3 + s^2(CL_2L_3 + L_2L_1 + L_2L_3 + L_1L_3) + L_2 + L_3 = 0 \tag{2}$$

where s is the complex Laplace variable. The roots of the fourth degree Equation (2) are composed of two pairs of complex conjugate frequencies:

$$\begin{cases} s_{1,2} = \pm j2\pi f_c \\ s_{3,4} = \pm j2\pi f_d \end{cases}$$

The charge transient frequency f_c is the lower positive imaginary part, i.e., $f_c = \mathrm{imag}(s_1)/(2\pi)$.

5. Results of the Analytical Algorithm Based on the Charge Transient Current Waveform

The proposed method is tested on a simulated 60 kV single circuit OHL, D = 60 km unearthed operated. OHL data are based on the "S60 type" pylon and are reported in Table 1. In the paper, EMTP-rv simulated fault currents are used in substitution of the real measurements. The sampling frequency is set to 100 kHz.

Table 1. Electrical Parameters and Position of Conductors in the Case Study.

	Section (mm^2)		$r_{20°}$	ℓ
	Ext.	Int.	(Ω/km)	(mH/km)
Conductor: ACSR	103.4	16.84	0.2819	0.03922
Ground wire: Steel		65.81	2.416	2
Line length (km)			60	
Conductor Positions				
	a)	b)	c)	0)
Conductor height from earth (m)	17.5	15	13	20
Conductor distance from pylon (m) [1]	1.6	−3.15	2.5	0

[1] the pylon axis is assumed as reference.

The simulated fault distance d_s, the "measured" frequency f_u, the calculated fault distance d_c, the absolute error Δ, and percentage one ε are reported in Table 2. The meanings of Δ and ε errors are the following:

$$\Delta = d_c - d_s$$

$$\varepsilon = 100 \cdot \frac{d_c - d_s}{D}$$

The error is "relatively" low only in the second portion of the line length (referred to as the fault locator position), whereas in the first portion, the error is high (see Figure 6). The average percentage error is 5.18%, whereas the worst is 13.9%. These errors are due to the simplifying hypotheses in the circuit modelling: having neglected the inductive mutual couplings between phases weights more in the first part of the line chiefly at one third of the line length (i.e., d_s = 20 km).

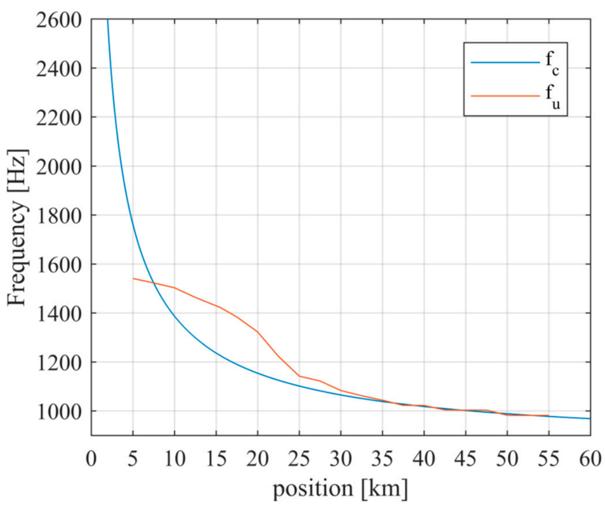

Figure 6. Comparison of "measured" frequency simulated by EMTP-rv and frequency calculated by a lumped parameter circuit.

However, the average error is too high, especially for the PsG short circuit occurring in the first portion of the line. In order to improve the algorithm accuracy, a twofold possibility yields:

✓ Creating a more accurate model, by using a distributed parameter circuit or by considering the effect of the mutual couplings;

✓ Studying the same phenomenon by means of a different approach (as performed in this paper).

Table 2. Calculated Error of the Fault Location by Analytical Method Applied to the Transient.

d_s (m)	f_u (Hz)	d_c (m)	Δ (m)	ε (%)
5000	1540.9	7194	2194	3.66
7500	1522.7	7435	−65	−0.11
10,000	1502.9	7740	−2260	−3.77
12,500	1463.6	8372	−4128	−6.88
15,500	1422.3	9162	−6338	−10.56
17,500	1383.6	10,010	−7490	−12.48
20,000	1322.2	11,660	−8340	−13.90
22,500	1222.9	15,600	−6900	−11.50
25,000	1142.2	20,090	−4910	−8.18
27,500	1122.3	22,740	−4760	−7.93
30,000	1083.5	27,270	−2730	−4.55
32,500	1062.2	30,540	−1960	−3.27
35,000	1043.9	34,030	−970	−1.62
37,500	1023	38,560	1060	1.77
40,000	1022.5	39,020	−980	−1.63
42,500	1004.2	44,350	1850	3.08
44,500	1003.2	44,560	60	0.10
47,500	1003.5	44,440	−3060	−5.10
50,000	982.3	52,890	2890	4.82
52,500	981.82	53,160	660	1.10
55,000	981.56	53,280	−1720	−2.87

Both possibilities have been investigated. Since a more complex model is characterized by an uncontrolled growth [7,30] of the dimensions of the characteristic equation (shown in Equation (2) in the Laplace domain), the authors moved towards the adoption of a different approach, i.e., the Artificial Neural Network-based algorithm. In the following, the computational capability of a machine learning-based algorithm is shown: a sensitivity analysis is proposed in order to assess the algorithm stability.

6. Artificial Neural Network-Based Algorithm

ANNs are biologically inspired computer programs designed to simulate the processing information technique of the human brain. ANNs gather their knowledge by detecting patterns and relationship in data and learn through "experience", not by pre-programmed code. An ANN consists of hundreds of single units, the artificial neurons, connected by "synapses" and organized in layers. A certain number of weighted inputs, a transfer function, and one output characterize each neuron. The weights are adjustable parameters during the learning phase. The weighted sum of various inputs is passed through a nonlinear transfer function, which determines the activation of the single neuron. During the training phase, the inter-unit connections are optimized until the error in prediction is minimized and the network reaches the specified level of accuracy. Once the network is trained and tested, it can receive new input information to predict the desired output (the fault position in this case) [12]. In terms of model specification, ANNs can combine both simulation-based and experimental data. Output performance improves in time by means of experimental data, collected from the real faults [31]. The behaviour of ANNs is conditioned by their architecture and the learning rules. In this paper, the "Multilayer Perceptron" (MLP) ANN structure is used. As it is well-known, an MLP is a class of feedforward ANN (see Figure 7 for the feedforward network used in this paper) that consists of at least three layers.

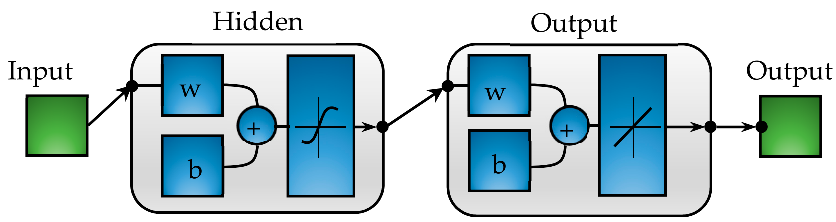

Figure 7. Feedforward neural network used in the paper.

In general, for fault location purposes, one hidden layer is sufficient for representing any given input/output relation, whereas the number of hidden neurons is equal to the single input vector dimension [13]. The single input vector is composed of a discretization of the transient current spectrum in the frequency range below 10 kHz, calculated by means of a t/f analysis. In this case, since a large portion of the frequency spectrum must be analysed, DFT [32] and DWT [33] are better than the CWT because of their lower computation times. The total datasheet is composed of 45 fault transient current spectra, and the fault currents have been simulated by means of EMTP-rv environment and processed in Matlab "Deep Learning" toolbox. The backpropagation method with the Levenberg-Marquart training algorithm is used. According to [34], with the aim of verifying network stability, in each training process, a small number of datasheet vectors are extracted to test the prediction ability in order to avoid the "over-fitting" problem. The training phase ends if the mean errors on the extracted vectors are smaller than a predetermined value. Once the training phase is completed, the network can be used to determine the faulty section. For power system application, it is intrinsically difficult to obtain a plentiful experimental-based datasheet and simulation-based ones could be not sufficiently accurate. Therefore, we decided to study the ANN response with a poor datasheet and some mathematical processes have been applied to maximize the output accuracy. Therefore, the process is iterated 150 times. A vector of possible fault distances is obtained and by calculating the average value, the worst solution is deleted. This process is iterated 100 times and the final fault distance is the average value of the 50 remaining outputs.

7. ANN-Based Algorithm Results

As already stated, the ANN algorithm is applied as an alternative to the analytical algorithm presented in Section 4: obviously, it is applied to the same case study of the previous section. The ANN-based algorithm results are reported in Table 3: the errors are lower than those of the analytical algorithm, with an average percentage value of 0.36% and a maximum value of 2.50%. Furthermore, it is worth noting that the percentage error is higher at both line ends. These results are predictable because of the datasheet configuration. In fact, it is composed of vectors which are equally spaced along the entire line length; therefore, if the fault occurs at the line ends, there is a lack of information exactly where more information is needed. This problem could be solved by increasing the datasheet dimension at both line ends. In Figure 8, the variation of the absolute value of the percentage error at each iteration is shown in blue, whereas the trend line, calculated by means of a quadratic fitting, is highlighted in red. The plot is calculated for the 12th case of Table 3. The percentage error decreases monotonously. If the iteration process was not applied, the maximum value of the percentage error would be equal to 4.45%. By applying the first iteration process, it decreases up to 0.48% and by applying the second one, it decreases up to 0.17%.

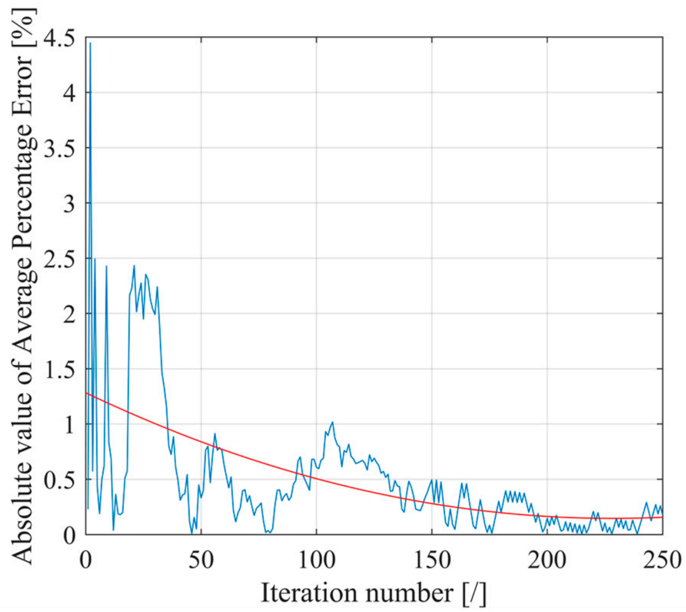

Figure 8. Variation of the percentage error with the iteration number for d_s = 32.5 km (12th rows of Table 3).

Table 3. Calculated Error of the Fault Location by an ANN-Based Algorithm.

d_s (m)	d_c (m)	Δ (m)	ε (%)
5000	6502	1502	2.50
7500	7520	20	0.03
10,000	9953	−47	−0.08
12,500	12,659	159	0.27
15,500	15,584	84	0.14
17,500	17,735	235	0.39
20,000	20,075	75	0.13
22,500	22502	2	0.00
25,000	25,012	12	0.02
27,500	27,463	−37	−0.06
30,000	29,970	−30	−0.05
32,500	32,581	81	0.14
35,000	34,978	−22	−0.04
37,500	37,472	−28	−0.05
40,000	39,990	−10	−0.02
42,500	42,676	176	0.29
44,500	44,499	−01	−0.00
47,500	47,551	51	0.09
50,000	50,727	727	1.21
52,500	52,502	2	0.00
55,000	53,798	−1202	−2.00

In order to confirm that the ANN-based algorithm is more accurate than the frequency response analytical one, Figure 9 shows the percentage errors vs fault distance for the frequency response analytical algorithm (blue line) and the ANN one (orange line).

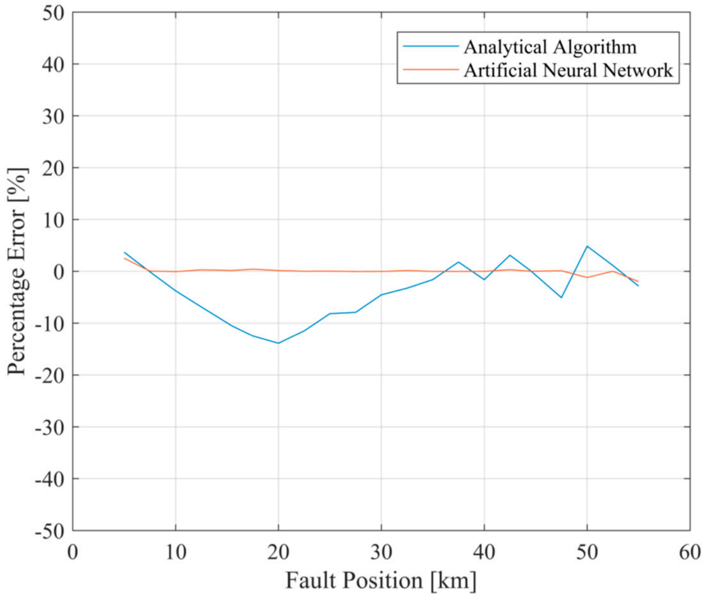

Figure 9. Percentage error vs fault distance for both algorithms.

8. Application to a Double-Circuit OHL

With regard to the algorithm stability, the algorithm response for different OHL configurations is presented. In the following, a double-circuit OHL configuration is considered. Line parameters are the same as those in Table 1, but the horizontal distance of the second three-phase line from the pylon is mirrored. In Figure 10, the charge loop (green) and the discharge loop (red) are highlighted with reference to the double-circuit OHL. The fault current spectra by varying the fault distances are reported in Figure 11: the frequency spectra for three different case studies (d_s = 2.5 km, 30 km, 57.5 km) are shown in the frequency range below 3 kHz.

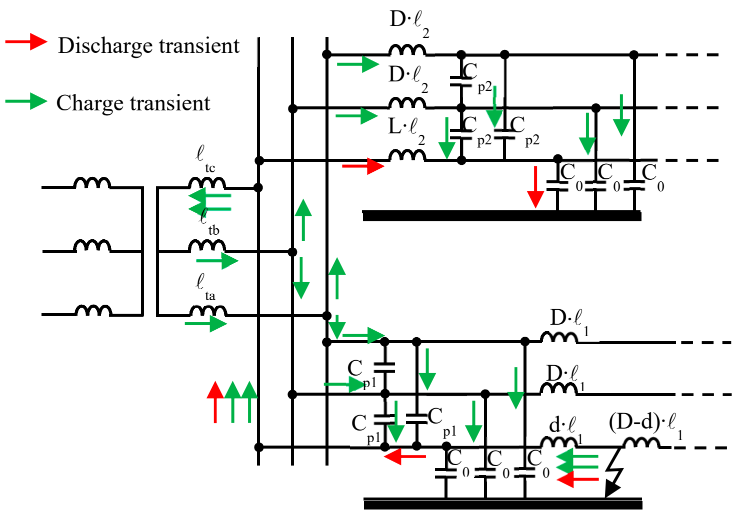

Figure 10. Charge and discharge transient circuits for a double-circuit OHL during a PtG fault (subscript 1 and 2 in the p.u.l. phase inductances refer to OHL 1 and OHL 2 and not to positive and negative sequence).

It is possible to infer from Figure 11 that a direct correlation between the fault position and the frequency components of the transient current does not exist; in fact, every frequency peak for different fault distances has the same abscissa. However, it is also possible to observe that every frequency component has different amplitudes for different fault distances. Therefore, the frequency response analytical algorithm (see Section 4) for this case study is not applicable; notwithstanding, the correlation between the y-axis values and the fault distance can be used for the training of the ANN algorithm. The ANN-based algorithm is developed in accordance with Section 6. In Table 4, the results of this second analysis are presented. A sensitivity analysis has been performed for different datasheet dimensions. The number of fault events remains constant (i.e., 45), but the discretization of the transient current spectra varies. The sensitivity analysis is performed in order to find the optimum condition between the accuracy and requested CPU time. It would be desirable, in fact, that the operators might start the fault clearance operations about 15–20 min after the fault occurrence. The presented results are obtained by an Intel®Core ™ i7-7700K CPU@4.2 GHz processor. Obviously, the CPU time of a more powerful processor is lower. Therefore, it is possible to obtain better results with the same CPU time.

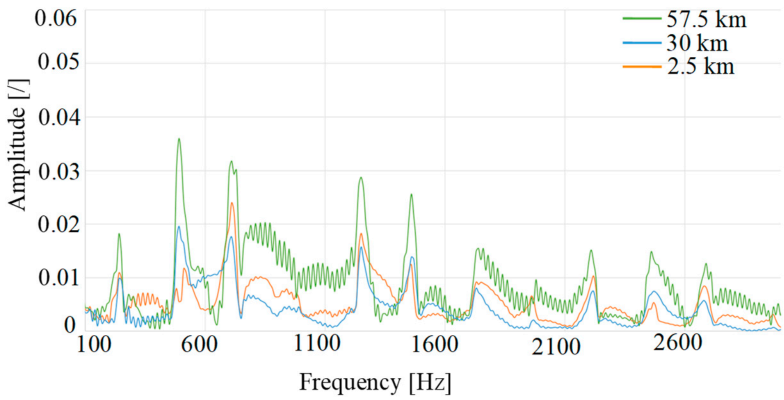

Figure 11. Transient current frequency spectra for different fault distances.

The results of the analysis of the ANN-based algorithm application are shown in Table 4. From Table 4, the percentage error is low, with a maximum value of 5.14% and an average percentage one of 0.65% only with high M.C.T. (about 62 min). By comparing the percentage error trend with the fault distance for the single-circuit OHL and double-circuit one, the maximum values of percentage error occur when the fault is located close to the line ends. This error is ascribed to the datasheet composition; in fact, it has a lack of information in the remote end portion of the line. It is possible to further reduce the percentage error by increasing the datasheet dimension for the aforementioned portion of the line with the obvious drawback of a CPU time increase. When due consideration is given to the real applicability of this ANN-based technique, it is worth highlighting that the training of ANN is always based on models derived in electro-magnetic software. Such shape of training implies the knowledge of all the data of the overhead line spans; heights at the towers; sags; and conductor types, including earth wires, if there are any. Even if this kind of application seems scientifically interesting, from industrial and engineering standpoints, it does not seem particularly straightforward for an extensive application of fault location in unearthed distribution networks.

Table 4. Double-circuit OHL: Fault Location Errors for ANN-based Algorithm for Different Datasheet Dimensions.

Datasheet Dimension	**45 × 45**			**45 × 30**			**45 × 15**		
d_s **(km)**	d_c **(km)**	**Δ (km)**	ε **(%)**	d_c **(km)**	**Δ (km)**	ε **(%)**	d_c **(km)**	**Δ (km)**	ε **(%)**
2.5	2818	318	0.53	3876	1376	2.9	3554	1054	1.76
5	5.036	0.036	0.06	8487	3487	5.81	8507	3507	5.85
7.5	7.605	0.105	0.18	9120	1620	2.70	9410	1910	3.18
10	10.65	0.65	1.1	11,453	1453	2.42	11,968	1968	3.28
12.5	15.58	3.08	5.14	14,289	1789	2.98	14,881	2381	3.97
15.5	14.91	−0.59	−0.98	16,234	1234	2.06	16,561	1561	2.60
17.5	17.52	0.02	0.04	18,810	1310	2.18	18,848	1348	2.25
20	20.05	0.058	0.10	21,124	1124	1.87	21,431	1431	2.39
22.5	22.48	−0.011	−0.025	23,814	1314	2.19	24,390	1890	3.15
25	25.20	0.208	0.35	26,285	1285	2.14	26,425	1425	2.38
27.5	27.55	0.058	0.10	27,896	396	0.66	28,018	518	0.86
30	29.74	0.252	−0.42	30,755	755	1.26	30,731	731	1.22
32.5	32.41	−0.081	−0.14	33,311	811	1.35	34,125	1625	2.71
35	34.88	−0.117	−0.2	36,791	1791	2.99	37,273	2273	3.79
37.5	36.64	−0.858	−1.43	38,778	1278	2.13	37,272	−228	−0.38
40	40.01	0.011	0.02	41,159	1159	1.93	41,409	1409	2.35
42.5	42.51	0.012	0.02	43,917	1417	2.36	43,466	966	1.61
44.5	44.57	0.074	0.12	45,328	328	0.55	44,993	−7	−0.01
47.5	47.45	−0.044	−0.07	47,011	−489	−0.82	46,868	−632	−1.05
50	49.44	−0.554	−0.92	51,531	1531	2.55	51,899	1899	3.17
52.5	52.27	−0.225	−0.38	52,852	352	0.59	52,644	144	0.24
55	56.21	1.212	2.02	56,635	1635	2.73	56,970	1970	3.28
A.P.E. [1] (%)		0.65			2.12			2.29	
M.C.T. [2] (s)		4955.91			759.68			137.42	

[1] A.P.E. is the average percentage error. [2] M.C.T. is the mean computation time.

9. Conclusions

In this paper, two different approaches for fault location estimation based on the study of charge transient capacitances are presented. The former is based on an analytical method based on the analysis of the charge transient current waveform: the average percentage error in locating a phase-to-ground short circuit is 5.18%, whereas the maximum one is 13.9%. They are too high, mainly when the OHL is located in mountainous territories. In the latter, the collected data from simulated short circuits in EMTP-rv are used to create the datasheet for the training of ANN implemented in the Matlab "Deep Learning" toolbox: the average percentage error in locating a phase-to-ground short circuit is 0.36%, whereas the maximum one is 2.50%. These errors are lower than those of the frequency response algorithm. Moreover, the ANN errors can be further decreased, even if with higher CPU times. Because of this high CPU time of the ANN-based algorithm, a last analysis is performed for different datasheet dimensions. The main purpose of the present work was to investigate the fault generated transient currents by means of two different approaches in order to highlight their strengths and weaknesses: the analytical method has greater errors with lower CPU times, whereas the ANN-based algorithm has smaller errors and higher CPU times.

In the near future, a measurement campaign is foreseen in a long overhead line with unearthed neutral located in a mountainous territory: only at that time, the presented algorithms will be validated. Moreover, the authors are investigating the applicability of these techniques to AC and DC cables [35–39].

Author Contributions: G.R. wrote a first draft of the paper and developed the models. R.B. reviewed the paper, acquired the founding resources, approved the final paper, and supervised the entire work. M.P. conceived the project.

Funding: This research was funded by TERNA-ENSIEL grant number ST 18 "Fault Location in un-earthed high voltage transmission grid".

Conflicts of Interest: The authors declare no conflict of interest.

Appendix A. Hilbert Transform (HT)

Typically, whenever a fault location algorithm is applied, two unknowns are present: the fault position and the fault impedance. In many algorithms, it is important to exclude fault impedance from calculations, because it is impossible to calculate it "a priori" [1]. HT can be applied for this purpose. The HT is one of the most important operators in the field of signal theory [10]. In this paper, the HT is applied to the spectral component of fault current referred to as the charge transient phenomenon. The main purpose of this transform consists of reproducing the "pre-envelope" signal from a real data sequence. Given a function *i(t)*, its HT $\underline{i}(t)$ is defined as

$$\underline{i}(t) = \frac{1}{\pi} PV \int_{-\infty}^{\infty} \frac{i(t)}{t-\tau} d\tau,$$

where *t* is the time interval, PV denotes the Cauchy principal value of the integral, and τ is the time constant of the signal. A general time data sequence *i(t)* and its HT define a complex function *I(t)*, as follows:

$$I(t) = i(t) + j\underline{i}(t)$$

which is called the analytic signal. The instantaneous angular frequency *ω(t)* of the analytic signal can be computed as

$$\omega(t) = \frac{d}{dt}\left[\arctan\left(\frac{\underline{i}(t)}{i(t)}\right)\right]$$

In this phase, it is important to introduce the concept of the damping factor α_n of *i(t)*. It is defined as the approximated slope of the function *i(t)* [7]:

$$\alpha_n = \frac{i_{pk}(t_n) - i_{pk}(t_{n+1})}{t_n - t_{n+1}} \tag{A1}$$

where i_{pk} represents the peak of the transient current, t_n is the time instant of the first studied current peak, and t_{n+1} is the time instant of the second current peak. By means of (A1), a vector of damping factors is obtained. It is possible to link every damping factor value to a proper angular frequency value ω_n, computed as the average value of the instantaneous angular frequency *ω(t)* in the time interval $t_n - t_{n+1}$. The un-damped frequency f_u can finally be computed as

$$f_u = \frac{\sum_n \sqrt{\alpha_n^2 + \omega_n^2}}{2\pi n}$$

References

1. Van der Sluis, L. *Transients in Power Systems*; Wiley & Sons: Hoboken, NJ, USA, 2001; ISBN 978-0-471-48639-8.
2. Baù, M.; Benato, R.; Sessa, S.D.; Poli, M.; Quaciari, C. Reti in Alta tensione a neutro isolato: Metodi per la rilevazione della distanza di guasto monofase. *L'Energia Elettr.* **2016**, *93*, 49–57.
3. Baù, M.; Benato, R.; Sessa, S.D.; Poli, M.; Quaciari, C. Review of the fault location methods for phase to ground short circuits in unearthed sub-transmission networks. *Int. Rev. Electr. Eng.* **2017**, *12*, 82–89.
4. Benato, R.; Sessa, S.D.; Poli, M.; Quaciari, C.; Rinzo, G. An on-line travelling wave fault location method for unearthed operated high voltage overhead line grids. *IEEE Trans. Power Deliv.* **2018**, *33*, 2776–2785. [CrossRef]

5. Benato, R.; Sessa, S.D.; Poli, M.; Quaciari, C.; Rinzo, G. Fault location in unearthed 60 kV subtransmission network based on the travelling wave method. In Proceedings of the 2017 AEIT International Annual Conference, Cagliari, Italy, 20–22 September 2017.
6. Zhang, W.; Xiao, X.; Wang, Y. Charging transient based SLG fault location in neutral unearthed distribution system. In Proceedings of the 2011 Asia-Pacific Power and Energy Engineering Conference (APPEEC), Wuhan, China, 25–28 March 2011.
7. Adzman, M.R.; Lehtonen, M. Fault location in MV unearthed distribution network using undamped frequency of the transient signal. In Proceedings of the 3rd International Conference on Energy, Environment, Devices, Systems, Communications, Computers (INEEE12), Rovaniemi, Finland, 18–20 April 2012.
8. Imris, P. Transient Based Earth Fault Location in 100 kV Subtransmission Networks. Ph.D. Thesis, Helsinky University of Technology, Helsinky, Finland, 2006.
9. Abdel-Fattah, M.F.; Lethonen, M. Transient algorithm based on earth capacitance estimation for earth fault detection in medium voltage networks. *IET Gener. Transm. Distrib.* **2012**, *6*, 161–166. [CrossRef]
10. Hanninen, S. *Single Phase Earth Faults in High Impedance Grounded Networks: Characteristics, Indication and Location*; Pubblication 453 VTT; Technical Research Centre of Finland: Espoo, Finland, 2001.
11. Jiang, B.; Shi, S.; Dong, X.; Wang, B. Single phase grounding fault location based on frequency domain characteristics of fault current. In Proceedings of the International Conference on Advanced Power System, Automation and Protection, Beijing, China, 16–20 October 2011.
12. Prasad, A.; Edward, J.B. Importance of Artificial Neural Networks for Location of Faults in Transmission Systems: A Survey. In Proceedings of the 11th International Conference on Intelligent Systems and Control (ISCO), Coimbatore, India, 5–6 January 2017; pp. 357–362.
13. Bashier EOmer, M.T.; Alrhirn, A.A. Transmission line faults detection, classification and location using artificial neural network. In Proceedings of the 2011 International Conference & Utility Exhibition on Power and Energy Systems: Issues and Prospects for Asia (ICUE), Pattaya City, Thailand, 28–30 September 2011; pp. 1–5.
14. Altuve, H.J.; Chacon, O.L.; Vazquez EPosadas, D.; Sanchez, E.N. Neural-network based fault location estimator for transmission line protection. In Proceedings of the ISAI/IFIS, Cancun, Mexico, 3–5 November 1996; pp. 186–191.
15. Tawfik, M.M.; Morcos, M.M. ANN-based techniques for estimating fault location on transmission lines using prony method. *IEEE Trans. Power Deliv.* **2001**, *16*, 219–224. [CrossRef]
16. Josè, A.C.B.; Costa, F.B.; Santos, W.; Neves, W.L.A.; Souza, B.A. High impedance fault location-case study using wavelet transform and artificial neural netuworks. In Proceedings of the 22th International Conference on Electricity Distribution, Stockholm, Sweden, 10–13 June 2013.
17. Zayandehroodi, H.; Mohamed, A.; Shareef, H.; Mohammadjafari, M. Determining exact fault location in a distribution network in presence of DGs using RBF neural networks. In Proceedings of the 2011 IEEE International Conference on Information Reuse & Integration, Las Vegas, NV, USA, 3–5 August 2011.
18. Dehghani, F.; Khodnia, F.; Dehghan, E. Fault location of unbalanced power distribution feeder with distributed generation using neural networks. In Proceedings of the 24th International Conference & Exihibition on Electricity Distribution (CIRED), Glasgow, UK, 12–15 June 2017.
19. Abdollahi, A.; Seyedtabaii, S. Transmission line fault location estimation by Fourier & Wavelet transforms using ANN. In Proceedings of the 2010 4th International Power Engineering and Optimization Conference, Shah Alam, Malaysia, 23–24 June 2010; pp. 573–578.
20. Tabatei, M.R.; Mosavi, M.R.; Farajiparvar, P. A travelling wave fault location technique for three terminal lines based on wavelet analysis and recurrent neural network using GPS timing. In Proceedings of the Smart Grid Conference, Tehran, Iran, 17–18 December 2013; pp. 268–272.
21. Lin, X.; Mao, P.; Weng, H.; Wang, B.; Bo, Z.Q.; Klimek, A. Study on fault location for high voltage overhead transmission lines based on neural network system. In Proceedings of the International Conference on Intelligent Systems Applications to Power Systems, Niigata, Japan, 5–8 November 2007; pp. 1–5.
22. Zhang, S.; Shang, W.J.; He, Z. A fault locating algorithm for the resonant grounding system based on the parameter identification under charge transient. In Proceedings of the Power and Energy Engineering conference, Shanghai, China, 27–29 March 2012.
23. Liu, P.; Huang, C. Detecting single-phase-to-ground fault event and identifying faulty feeder in neutral ineffectively grounded distribution system. *IEEE Trans. Power Deliv.* **2018**, *33*, 2265–2273. [CrossRef]

24. Prasad, C.G.D.; Prasad, D.J.V. Fault detection and phase selection using Euclidean distance based function for transmission line protection. In Proceedings of the International Conference on Advances in Electrical Engineering (ICAEE), Vellore, India, 9–11 June 2014.
25. Addison, P.S. *The Illustrated Wavelet Transform Handbook*; Institute of Physics: London, UK, 2002; ISBN 0750306920.
26. Biswal, S.; Biswal, M.; Malik, O.P. Hilbert Huang transform based online differential relay algorithm for shunt compensated transmission line. *IEEE Trans. Power Deliv.* **2018**, *33*, 2803–2811. [CrossRef]
27. Serra, H.; Oliveira, J.P.; Paulino, N. A 50 Hz SC notch filter for IoT application. In Proceedings of the IEEE International Symposium on Circuits and Systems (ISCAS), Baltimore, MD, USA, 28–31 May 2017.
28. Borghetti, A.; Bosetti, M.; di Silvestro, M.; Nucci, C.A.; Paolone, M. Distribution power networks: Definition of mother wavelets inferred from fault originated transients. *IEEE Trans. Power Syst.* **2008**, *23*, 380–388. [CrossRef]
29. Moravej, Z.; Movahhedneya, M.; Radman, G.; Pazoki, M. Effective fault location technique in three-terminal transmission line using Hilbert and discrete wavelet transform. In Proceedings of the IEEE International Conference on Electro/Information technology (EIT), Dekalb, IL, USA, 21–23 May 2015.
30. Adzman, M.R. Earth Fault Distance Computation Methods Based on Transients in Power Distribution Systems. Ph.D. Thesis, Aalto University, Aalto, Finland, 2014.
31. Vasanth, S.; Yeap, Y.M.; Ukil, A. Fault Location Estimation for VSC-HVDC System Using Artificial Neural Network. In Proceedings of the IEEE Region 10 Conference (TENCON), Singapore, 22–25 November 2016.
32. Mamis, M.S.; Arkan, M. FFT based fault location algorithm for transmission lines. In Proceedings of the International Conference on Electrical and Electronics Engineering, Bursa, Turkey, 1–4 December 2011.
33. Singh, S.; Vishwakarma, D.N. Application of DWT and ANN for fault classification and location in a series compensated transmission line. In Proceedings of the IEEE 6th International Conference on Power Systems, New Delhi, India, 4–6 March 2016.
34. Braspenning, P.J.; Thuijsman, F. *Artificial Neural Networks: An Introduction to ANN Theory and Practice*; Springer: Berlin/Heidelberg, Germany; New York, NY, USA, 1995; ISBN 3-540-59488-4.
35. Benato, R.; Forzan, M.; Marelli, M.; Orini, A.; Zaccone, E. Harmonic behaviour of HVDC cables. *Electr. Power Syst. Res.* **2012**, *89*, 215–222. [CrossRef]
36. Benato, R.; Paolucci, A. Multiconductor cell analysis of skin effect in Milliken type cables. *Electr. Power Syst. Res.* **2012**, *90*, 99–106. [CrossRef]
37. Benato, R.; Dambone Sessa, S.; Guglielmi, F.; Partal, E.; Tleis, N. Ground Return Current Behaviour in High Voltage Alternating Current Insulated Cables. *Energies* **2014**, *7*, 8116–8131. [CrossRef]
38. Benato, R.; Dambone Sessa, S. A New Multiconductor Cell Three-Dimension Matrix-Based Analysis Applied to a Three-Core Armoured Cable. *IEEE Trans. Power Deliv.* **2018**, *33*, 1636–1646. [CrossRef]
39. Benato, R.; Sessa, S.D.; Forzan, M. Experimental Validation of 3-Dimension Multiconductor Cell Analysis by a 30 km Long Submarine Three-Core Armoured Cable. *IEEE Trans. Power Deliv.* **2018**, *33*, 2910–2919. [CrossRef]